Rotor Noise Due to Atmospheric Turbulence Ingestion—Part I: Fluid Mechanics

J. C. Simonich,* R. K. Amiet,† and R. H. Schlinker‡
United Technologies Research Center, East Hartford, Connecticut
and
E. M. Greitzer§
Massachusetts Institute of Technology, Cambridge, Massachusetts

An analysis has been developed to predict helicopter rotor noise due to ingestion of turbulence. The method incorporates an upstream isotropic turbulence model and a (rapid distortion) turbulence contraction description to determine the statistics of the anisotropic turbulence at the rotor plane. An important feature of the contraction process is the differential drift of fluid particles on adjacent streamlines, which leads to tipping and stretching of the vortex filaments associated with the turbulence. The analysis is applied to a main rotor operating in atmospheric turbulence. For mean-flow contraction ratios representative of hover and low-speed forward flight and vertical ascent, computations are carried out to show that accurate prediction of the vorticity components and hence nonisotropic turbulence at the rotor face requires accounting for this differential drift. A companion paper,[1] presented as Part II, describes the rotor acoustic model and the resulting atmospheric turbulence ingestion noise prediction based on the method. Although the predictions in both papers are limited to atmospheric turbulence, the method is applicable to isotropic upstream turbulence fields undergoing generalized distortions.

Nomenclature

C_T = rotor thrust coefficient $= T/\rho\pi R^2(\Omega R)^2$
e = unit vector along one of the three upstream or downstream axes
$E(k)$ = wave-number energy spectrum
g = gravitational acceleration
k = wave number
$\boldsymbol{k}$ = wave vector of turbulence
L_w^x = integral length scale
n = direction of the principle normal to the streamline
q,Q = velocity field and magnitude of a Fourier component of turbulence
R = rotor radius
T = thrust
u = turbulence fluctuation
U = local time mean velocity
U_∞ = mean horizontal freestream velocity
V_∞ = mean vertical freestream velocity
V_0 = rotor-induced velocity $= C_T\Omega R/2\sqrt{\lambda^2+\mu^2}$
v = vertical turbulence fluctuations
$\sqrt{\overline{v^2}/U_\infty}$ = rms turbulence intensity
x_i = upstream Cartesian coordinate system, $i = 1,2,3$
X = vector location
Z = height above ground
α = rotor tip path plane angle of attack
ϵ_{ijk} = alternating tensor
λ = wavelength of Fourier component of turbulence, or rotor inflow ratio $= (U_\infty \sin\alpha - V_0)/\Omega R$
μ = rotor advance ratio $= U_\infty \cos\alpha/(\Omega R)$
ξ_i = downstream Cartesian coordinate system
ρ = density
χ = wake skew angle $= \tan^{-1} \times [-U_\infty \cos\alpha/(U_\infty \sin\alpha - V_0)]$
ω,Ω = rotation rate
ω,Ω = vorticity field and magnitude of a Fourier component of turbulence [see Eq. (6)]

Subscripts

i,j,k = specify either a vector (such as one of the vectors e_1, e_2, e_3) or a 1, 2, 3 component of a vector (such as the first Cartesian component of the vector e_2)

Superscripts

U,D = upstream or downstream location, respectively

Introduction

NOISE produced by a helicopter represents the sum of the contributions of a number of separate noise sources. The list of possible rotor noise mechanisms is lengthy but in the absence of impulsive noise, broadband noise can be an important contribution.[2,3] Design of helicopters with reduced broadband noise level requires the ability to predict the contribution from each broadband noise mechanism.

A specific noise source for which prediction methods have been developed is the ingestion of turbulence by rotor blades; however, the earlier predictions assumed isotropic turbulence at the rotor disk. (See Part II for a review of the previous noise analyses.) The methods thus do not yield realistic sound pressure levels and acoustic spectra for rotors operating in a turbulence field with a nonisotropic spectrum. Although a generalized acoustic analysis existed, the turbulence conditions at the rotor face, which are the inputs to such an analysis, were not accounted for. The primary limitation was the lack of a rigorous description of the distortion of the turbulence as it is ingested into the rotor.

Considering these limitations relative to a main rotor operating in a turbulent atmosphere, the absence of realistic models of the initial turbulence and its distortion during ingestion

Received Sept. 16, 1986; revision received May 27, 1989.

*Research Engineer, Aeroacoustics and Gas Dynamics Research. Member AIAA.
†Senior Research Engineer, Aeroacoustics and Gas Dynamics Research. Member AIAA.
‡Supervisor, Aeroacoustics and Gas Dynamics Research. Member AIAA.
§Professor and Director of Gas Turbine Laboratory. Member AIAA.

makes it difficult to rank this particular turbulence ingestion noise relative to other noise mechanisms. Direct assessment from full-scale tests is not possible since other operative noise mechanisms are present. There is thus a need to incorporate improved descriptions of the atmospheric turbulence field and the effect of the ingestion on the turbulence characteristics at the rotor disk into an overall prediction scheme, and this is the objective of the present study.

Scope of the Overall Problem

Before describing the flow details, we briefly discuss the scope and formulation of the general problem. To develop a calculation procedure for rotor noise due to turbulence ingestion, several different phenomena must be modeled: 1) spectral distribution of the upstream turbulence (ambient turbulent vorticity field), 2) background (mean) flow into the rotor (the flow that convects the turbulent vorticity), 3) distortion of the turbulence as it is ingested into the rotor, 4) unsteady surface pressures generated on the blades due to the unsteady flow that the rotor experience, and 5) acoustic radiation resulting from the fluctuating surface pressures. Here the ambient turbulent field, which represents the input to the prediction, has been specified as atmospheric turbulence. However, other unsteady velocity fields can be specified.

The overall calculation process is indicated schematically in Fig. 1. The computations of 2 and 3 can be regarded as a transfer matrix which converts the ambient turbulence field to the rotor inlet turbulence field. The computations in 4 link the turbulence conditions with the resulting noise in 5.

Methodology

The paper covers some quite different topics, namely, the several different components comprising the overall procedure, and organization is also in terms of these components. The present paper (Part I) deals with the fluid dynamic (rather than acoustic) aspects of the analysis represented by items 1, 2, and 3 in Fig. 1. The discussion begins with the selection of a realistic model for the atmospheric turbulence based on a critical assessment of existing experimental data. Following this, the mean-flow calculation and the streamline-tracing procedure are discussed, and numerical examples are given. The turbulence distortion model is then presented along with a clear statement of the assumptions in the description of the turbulence. The numerical approach for computing the turbulence components at the rotor face, based on numerical tracking of the vortex filaments comprising the unsteady flow, is included. Calculations are compared with the results based on classical theories of rapid distortion to indicate the range of parameters over which the latter cease to give an adequate representation of the rotor face turbulence. Numerical results are presented here also to illustrate the magnitude of the effects that are modeled.

Atmospheric Turbulence Model

Reviews of Previous Work

Recent review articles on the structure of the atmospheric boundary layer, reported by Teunissen,[4] Snyder,[5] and Fairall et al.,[6] show a large range of differences in the data reported as well as in proposed prediction methods, indicating that atmospheric modeling is not yet an exact science. The model presented here was chosen after a critical review of current literature and is representative of the current state of the art. Many of the correlations are based on Ref. 5 since it was the only model including nonneutral stability effects, which must be included to properly model the atmosphere when heat transfer is important.

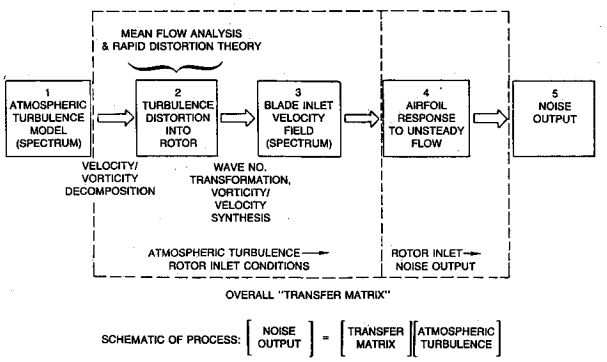

Fig. 1 Modules in overall prediction scheme.

Model Assumptions and Limitations

1) The flow is statistically stationary. This assumption has been shown to be valid for times on the order of 10–20 min,[4] which is two orders of magnitude more than the rotor inflow particle transit time.

2) The flow is homogeneous in any horizontal plane. Although strictly valid only for a homogeneous terrain, this assumption can be employed for terrain where the horizontal length scale of the variation in height or roughness length is much larger than the boundary-layer thickness.

3) The "ambient" turbulence is isotropic. The atmospheric boundary layer is a shear flow and hence not truly isotropic. The degree to which the atmospheric turbulence can be regarded as isotropic depends on the wave number considered; the assumption is valid for wave numbers in the inertial subrange and above. Wavelengths of interest in the present study are bounded by rotor diameter and blade thickness. Eddies larger than the diameter affect the rotor only as a slowly varying mean velocity, whereas eddies smaller than the airfoil thickness are not addressed by the acoustic source model. The wave-number range corresponding to these limits for a typical helicopter under neutrally stable atmospheric conditions is shown in Fig. 2. For this case, the wave numbers of interest are within the inertial subrange where the turbulence is primarily isotropic.

A full description of the procedure used to calculate the various parameters is given in Ref. 7, which can be referred to for the details of the model. The most important parameters for the calculation of the turbulence ingestion noise are the spectra $E(k)$ and the integral length scale L_w^x. As an illustration of the type of effects that have been examined, Fig. 2 indicates the spectrum that would be observed at heights Z of 50, 120, and 150 m, respectively. Over the wave-number range relevant to atmospheric turbulence ingestion noise, the turbulence spectra are nearly invariant with altitude.

Mean-Flow Computation

General Approach

To calculate the distortion of the turbulence field as it convects toward the rotor a description of the mean, or back-

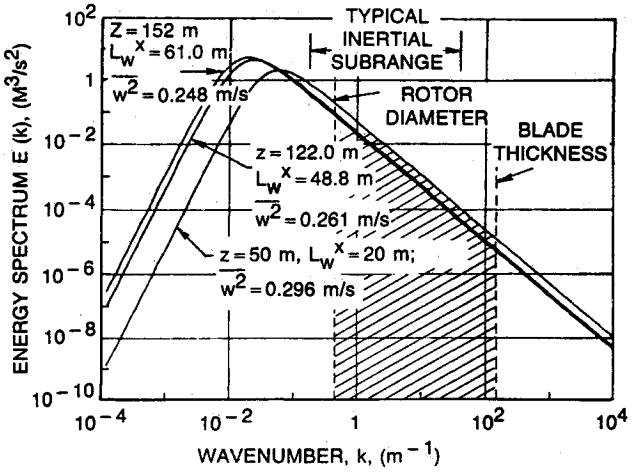

Fig. 2 Energy spectrum for wave-number range of interest on typical helicopter rotor.

Table 1 Helicopter Flight Conditions

Case	$U_\infty/\Omega R \times 10^2$	$V_\infty/\Omega R \times 10^2$	μ	$V_0/\Omega R \times 10^2$	α, deg	χ, deg
*FF*1	11.0	0.0	0.11	1.55	−2.3	79.7
*FF*2	4.89	0.0	0.049	3.12	−0.2	57.4
HOV	1.41	0.0	0.014	4.22	0.0	57.4
V1	0.0	0.835	0.0	5.17	0.0	18.5
*V*2	0.0	1.68	0.0	6.01	0.0	0.0
*V*3	0.0	3.35	0.0	7.69	0.0	0.0

$\Omega R = 182$ m/s, $R = 3.854$ m, $C = 0.244$ m, $C_T = 0.00377$

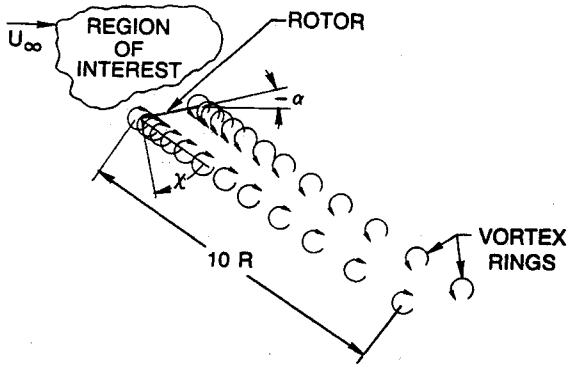

Fig. 3a Schematic of wake model.

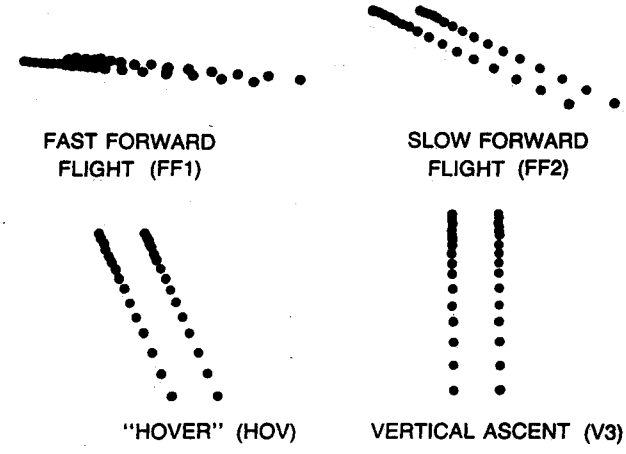

Fig. 3b Ring vortex wake model for various flight conditions.

ground flow, into the rotor is needed. The approach taken here is to develop an approximate method which retains the physical aspects of the problem that are most important.

Many existing helicopter aerodynamic analyses are concerned with the details of the flow downstream of the rotor, for example, the structure of the trailing vortex system.[8,9] For the present problem, however, it is the flow upstream of the rotor that is of interest and is controlled by the overall wake properties,[10] rather than the detailed wake structure. These considerations form the basis of the analytical approach to the mean-flow computation.

The mean flow upstream of the rotor can be taken as irrotational, and to calculate it, one can thus represent the wake by a number of discrete vortex rings. The velocity vector at any point is that induced by these vortex rings plus the ambient flight velocity. Although individual rings are axisymmetric, the skewed wake geometry that occurs in all cases other than pure vertical ascent results in a three-dimensional flowfield.

In the present study, 20 vortex rings were used with spacing varied so that the vortex separation distance was smaller near the rotor disk, as shown schematically in Fig. 3a. (Circulation per unit length along the wake is constant.) The vortices extended to approximately 5 (rotor) diam along the line of the wake. Computations showed that this was sufficiently far downstream to cause only a small effect on the flow upstream of the disk. Actual positions of the vortex rings for the cases investigated are shown in Fig. 3b; these will be discussed more fully below. All the ring vortices were the same diameter so that wake distortions are neglected. This affects the flow locally, but the overall character of the upstream velocity field should not be significantly altered.[10]

The wake skew angle χ (between the normal to the rotor disk and the wake boundary) is based on experimental measurements. The vortex strength was found by matching the induced velocity at the rotor face with experimental measurements,[9] for cases FF1 and FF2 in Table 1. For other operating points, the induced velocity was computed from overall momentum considerations for the rotor disk.[7]

Once the vortex wake strength is determined, the induced velocity at any point in the flowfield is found by summing the velocities induced by the vortex rings. The velocity field for an individual ring can be expressed in terms of elliptic integrals.[11] Details of the calculation are given in Ref. 7, and accurate expressions for evaluating the elliptic integrals of the first and second kind can be found in Ref. 12.

Since the wake skew angle was determined from data (rather than through a solution procedure which imposed no normal velocity at the wake boundary), an evaluation of the vortex ring wake model was also carried out.[7] The results showed that there was very little flow though the interface line formed by the vortex rings,[7] and hence the wake skew angle is indeed chosen in a consistent manner.

Streamline Tracing Procedure

Once the velocity field is known, the mean streamlines can be computed by integrating the equations that define the local streamline directions:

$$\frac{dx}{dt} = u(x,y,z) \tag{1}$$

$$\frac{dy}{dt} = v(x,y,z) \tag{2}$$

$$\frac{dz}{dt} = w(x,y,z) \tag{3}$$

These three coupled ordinary differential equations are numerically integrated, starting at a specified initial position, to give coordinates of any streamline. The method used adjusts the step size to control the local error so that larger steps can be taken in regions where the velocity gradients are small.[13]

In carrying out the computations, the primary interest is in streamlines which pass through the rotor disk since it is only the fluid particles on these streamlines that the rotor sees. Because the upstream location of these streamlines is not known a priori, it was more convenient to begin the calculation at desired locations on the rotor disk and integrate upstream, i.e., backwards in time. The computations were stopped when the streamlines passed outside of a cube 3 rotor diam on a side, centered on the rotor, since the streamlines are

then very close to parallel and the velocity is essentially uniform.

Definition of Rotor Operating Conditions to be Examined

Computations have been carried out for hover, vertical ascent, and forward flight. The conditions examined are given in Table 1. Not all of the numerical results are presented in this paper, and further information is given in Ref. 7. Figure 3b shows the locations of the ring vortices for four of these cases with the operating conditions chosen to match experimental data reported in Ref. 9.

Before the results are described, a precise definition of the hover condition is required. Here, hover refers to situations in which the aircraft is stationary relative to the ground. The "conditions at infinity" in hover are thus determined by the ambient wind, which was selected to be 5 kt (2.57 m/s), and the mean flow in hover is not axisymmetric but three dimensional. In fact, a mean wind is an important physical requirement for generating the fluid shear responsible for the atmospheric turbulence.

This definition of hover, which is appropriate to model test specifications, removes a potential source of ambiguity associated with the ambient level of turbulence. Turbulence intensity is specified as a fraction of the mean velocity. If the aircraft moves at the mean wind speed (instead of being stationary), the velocity far from the rotor would be zero. In this case, the fundamental assumptions on which the turbulence ingestion model described later are based (turbulent velocities much smaller than mean velocities) would not be valid. In addition, the contraction ratio (mean velocity at the rotor disk divided by mean velocity far upstream) is infinite. There is no real collection of methods that have been developed for dealing with such flows, and we have excluded this singular situation from consideration.

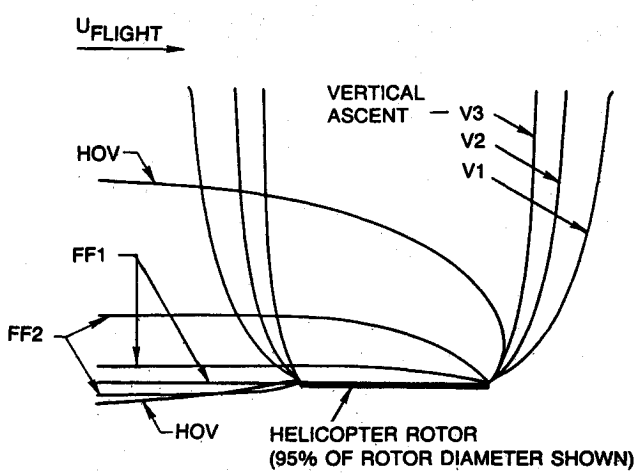

Fig. 4 Streamline envelope in vertical plane through centerline for six different operating conditions.

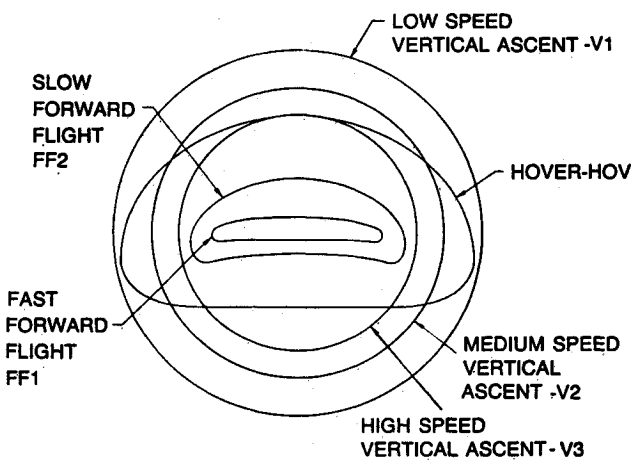

Fig. 5 Capture surfaces for six different operating conditions.

Numerical Results

Changes in the overall mean-flow features with operating conditions are indicated in Figs. 4 and 5. Figure 4 shows the projection of the "capture surface" (the dividing stream surface between fluid that passes through the rotor disk and fluid which does not) on the vertical plane of symmetry through the center of the rotor for the six cases of Table 1. The capture surface is based on streamlines which pass through a circumference at 95% of the rotor since the computation cannot be used to predict velocity very close to the blade tip which coincides with the vortex ring location. Substantial changes occur in the contraction ratio (upstream capture area/rotor disk area), and there is significant alteration in the basic streamline shapes as the operating condition changes.

Figure 5 presents a different view of the capture surface dependence on operating condition. This figure shows the projection of the capture surface onto a plane normal to the flow "at infinity" for the six conditions. In both Figs. 4 and 5, the strong asymmetry of the forward flight cases is evident. These cases cover a range of streamline configurations from no turning and no stream-tube contraction to high contraction and large turning, thus bounding the range of practical interest.

Figure 6 presents four different views of the streamlines and time lines (material lines) for the hover case (other cases are shown in Ref. 7). Here the material lines represent vortex filaments. View a shows the streamlines (solid lines) and material lines or time lines (dashed lines) on a vertical plane parallel to the velocity at infinity and passing through the center of the rotor disk. Views b, c, and d show three different viewing angles of the same streamlines which pass through a circumference at 95% of the rotor: b shows a top view, c a front view, and d a three-dimensional perspective view from an observer location 20 deg above and 70 deg from the ambient wind velocity direction. Turning and stretching of the material lines can be seen. At the far upstream location, material lines are orthogonal to the streamlines. Near the rotor, however, the material lines are tipped into the local streamwise direction, due to differences in velocity and in distance traveled for different fluid element streamlines. This differential drift time between streamlines has important implications for the evolution of the turbulence, as will be seen in the next section.

Turbulence Distortion Model

Selection of Analytical Model

In developing a description of the evolution of the atmospheric turbulence as it is convected toward the rotor, a basic

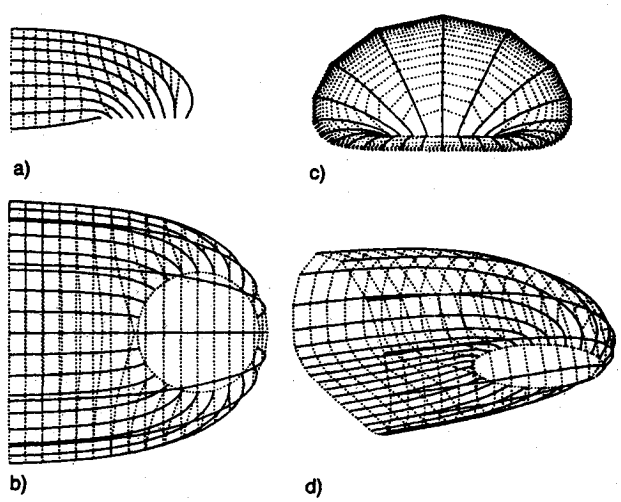

Fig. 6 Streamlines and timelines for hover case.

conceptual question rises concerning the detail needed in the analytical model. The answer depends not only on the application of the analysis but also on computational capabilities. As discussed in Ref. 7, an approximate turbulence model which is viewed as having the required accuracy is that of rapid distortion theory, which has been applied successfully to calculations of turbulent flow in many different situations. The velocity field is thus modeled as a primary flow, induced by the rotor, which convects (and distorts) the vortex filaments that represent the turbulence. If viscous effects can be neglected, it then suffices merely to know where the particles start and end along mean-flow streamlines. Since the vortex lines are also material lines, the previously described material line calculations can be used in conjunction with the Cauchy equations to describe the vorticity evolution and hence the turbulent vorticity field.

Using this approach, rapid distortion theory can account for the inherently three-dimensional process of vortex stretching and tilting, which can change both the frequency distribution and intensity of the turbulence. A further advantage of using this approach is that the consequences of the assumptions made can be evaluated and directly assessed relative to other physical models employed in the overall analysis.

Assessment of Approximation and Assumptions in Analytical Model

The approximations made in using rapid distortion theory can be illustrated using the equations for the rate of change of vorticity in a uniform density fluid. If the velocity field is composed of an irrotational mean flow, denoted by U, and a perturbation, which represents the turbulence, the vorticity transport equation can be written as

$$\boxed{\frac{D\omega'}{Dt} = (\omega' * \nabla)U} + (\omega' * \nabla)u' + \nu\nabla^2\omega' \qquad (4)$$

(I) (II)

In Eq. (4), the primed variables denote the velocity and vorticity of the turbulence. The terms within the dashed lines are those considered in rapid distortion theory, with (I) and (II) being associated with nonlinear effects (convection of perturbation vorticity by perturbation velocity), and viscous effects, respectively.

The first extensive quantitative applications of rapid distortion theory were by Ribner and Tucker[14] and Batchelor and Proudman.[15] In recent years, there have been several new approaches to the topic that have overcome several deficiencies of the earlier analyses, notably the treatments by Goldstein[16,17] and by Hunt.[18,19] The former is a very general analysis based on a new velocity field decomposition procedure which has several attractive features. Reference 19 gives a detailed discussion of these analyses.

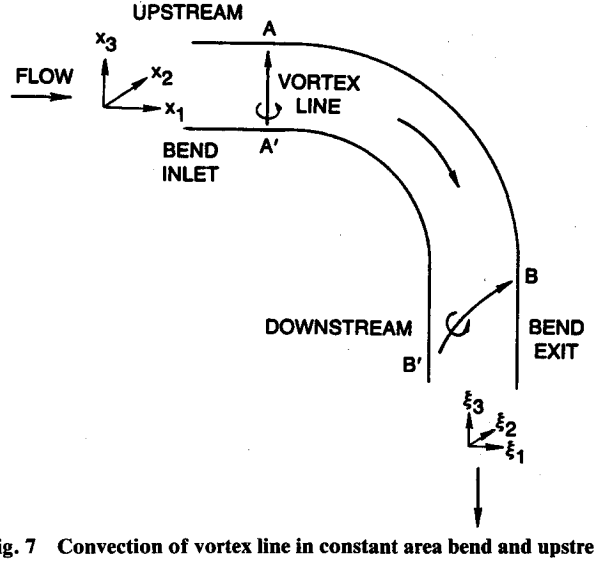

Fig. 7 Convection of vortex line in constant area bend and upstream and downstream coordinate system used in analysis.

As reported in Ref. 7, a shortcoming of the early analyses of Ref. 14 and an effect sometimes still not included in computations of turbulence evolution is the neglect of differential particle drift. (Drift time is the length of time for a fluid particle to be convected along a streamline from an upstream to a downstream station.) Using this approach, the only alteration of the turbulence is due to stream-tube area change. In general, however, the turbulence vorticity field can be distorted even if no stream-tube area change occurs as illustrated in Fig. 7, which shows a vortex filament being convected through a constant area bend. The line AA′ represents the vortex filament at a location upstream of the bend, while BB′ describes the filament at the downstream location. If the mean flow is irrotational, fluid particles on the inside of the bend have a smaller distance to move and travel faster than those on the outside. Particles at B will thus lag those at B', and the vortex line, which is a material line, will be rotated into the streamwise direction. This implies an increase in the vortex filament length, and hence an increase in the magnitude of the vorticity vector.

Production of streamwise vorticity and intensification of the vorticity magnitude is associated with the time history of the fluid particles and does not depend on the scale of the turbulence. There are, however, other effects which do depend on this scale arising from 1) spatial nonuniformity of the vorticity field and 2) interaction of the vortical flowfield with the boundaries.

The first of these implies that the simple vorticity/velocity relation for a homogeneous vorticity distribution no longer holds, and one must compute the contribution to the perturbation velocity from vortex elements over all space. In practice, this means that the integration must be taken over a scale considerably larger than the scale of the turbulence. Only for small turbulence scales (compared to the scale of the contraction) can the velocity/vorticity relation at any point therefore be regarded as the same as that which would exist in a homogenous flow having that distribution of vorticity.

The second point is that for a general vorticity field, irrotational velocity perturbations will arise due to the presence of the boundary. This interaction should be taken into account at distances from the boundary of less than the scale of the turbulence.

An assumption of this study is that the turbulence length scales are less than the scale of the contraction. Integral length scales in the atmospheric boundary layer are typically many times larger than the rotor diameter. However, the turbulence field is composed of eddies of various lengths. For wave-number components of the turbulent field which are of most interest for noise generation, the length scales will be less than the scale of the contraction. Eddies larger than the rotor appear only as slowly varying changes in the mean flow. Features of the turbulence ingestion process which are dependent on scale are thus not treated.

A final aspect of the present analysis is that viscous effects on the turbulence are neglected. Justification for this is given in Ref. 7, where an examination of the degree to which the assumptions of the theory are valid is also detailed.

Velocity Field and Spectrum of Turbulence Undergoing a Rapid Distortion

The evolution of the turbulence as it is convected toward the rotor includes changes in both the vorticity and wave vectors which characterize the local spectrum of the turbulence. A turbulent velocity field for incompressible flow can be expressed as a distribution of vorticity. For inviscid, constant density flow, vortex lines move with the fluid, and deformation of the fluid implies analogous deformation of the vortex lines. For the contractions of interest which have length and

width comparable (due to the irrotationality of the mean flow), there will not only be stretching (or compression) of the vortex lines but also tilting into directions different from the initial ones.

To analyze this, one can use the general expression due to Cauchy[20] for change in vorticity. The vorticity at the downstream (rotor face) station to that occurring at an upstream station along the same streamline is

$$\Omega_i^U = \Omega_j^D \frac{\partial x_i}{\partial \xi_j} \tag{5}$$

$$\Omega_i^D = \Omega_j^U \frac{\partial \xi_i}{\partial x_j} \tag{6}$$

In effect this is just the local application of the Helmholtz vortex theorems. The superscripts U and D denote upstream or downstream conditions, respectively, and, as shown schematically in Fig. 7, x_i represents the upstream coordinate system and ξ_i represents the downstream coordinate system. (Although the coordinates are shown with respect to the constant area bend, the nomenclature applies to the general situation.) The derivative $\partial x_i/\partial \xi_j$ is called the deformation tensor since it is directly related to the deformation of a given volume of fluid as it moves from upstream to downstream. Within rapid distortion theory, Eqs. (5) and (6) are linearized in that the deformation tensor is based on the mean-flow velocity field only.

To evaluate the deformation tensor for the three-dimensional flows under consideration, the streamline tracing procedure described previously is used. Starting at a given point on the rotor face, the equations describing the streamline coordinates are numerically integrated from the rotor face to a station far upstream for one streamline. Three other streamlines, displaced distances $d\xi_1$, $d\xi_2$, and $d\xi_3$ from the starting location are then also traced for the same time interval as the first. At the upstream "end" of the streamlines, a vector drawn from the end of the first streamline to the end of each of the others determines three of the nine components of the deformation tensor. Carrying out the procedure for $d\xi_1$, $d\xi_2$, and $d\xi_3$ yields all the nine components, written as $(\partial x_i/\partial \xi_j)$, and the matrix can be inverted to give the required quantities $(\partial \xi_i/\partial x_j)$.

The derivative evaluations involves a simple first-order scheme. However, trial runs showed that the desired accuracy could be achieved by taking small values of the distances $d\xi_1$, $d\xi_2$, and $d\xi_3$, typically 0.0001 radius. Other approaches such as writing the equations for the rate of change of the deformation tensor and integrating this numerically along a streamline are certainly possible, but are not necessary.

The transformation from the turbulent field upstream to downstream involves two vector quantities, the velocity and wave vector of a given Fourier component of the turbulence. Transformation of both of these is based on vortex lines being convected by the mean flow. The transformations are outlined in the following; a full description is given in Ref. 7.

Relations Between Vorticity and Velocity at a Point

The spectrum of turbulence is described in terms of Fourier gust components. For a single Fourier component, the velocity and vorticity fields are

$$q(\boldsymbol{k},\boldsymbol{x}) = \boldsymbol{Q}(\boldsymbol{k})e^{i\boldsymbol{k}\boldsymbol{x}} \tag{7}$$

$$\omega(\boldsymbol{k},\boldsymbol{x}) = \boldsymbol{\Omega}(\boldsymbol{k})e^{i\boldsymbol{k}\boldsymbol{x}} \tag{8}$$

The vector $\boldsymbol{k}$ is the wave vector, and $\boldsymbol{Q}$ and $\boldsymbol{\Omega}$ are the amplitudes of the velocity and vorticity field for the gust component.

If the definition of vorticity ($\omega = \nabla \times q$) is used together with the condition of solenoidality of the velocity field, the following (equivalent) relations can be derived between Fourier components of velocity and vorticity

$$\boldsymbol{\Omega} = i\boldsymbol{k} \times \boldsymbol{Q} \tag{9}$$

$$\boldsymbol{Q} = i\boldsymbol{k} \times \boldsymbol{\Omega}/k^2 \tag{10}$$

Relation Between Upstream and Downstream Velocities

If Eqs. (5), (9), and (10) are combined, the following relation between the upstream and downstream velocities is obtained:

$$Q_i^U(\boldsymbol{k}^U) = -(k_j^U/k^{U2})\, k_l^U Q_m^D(\boldsymbol{k}^D)\, \epsilon_{lmn} \frac{\partial x_k}{\partial \xi_n} \epsilon_{ijk} \tag{11}$$

Equation (11) relates upstream and downstream Fourier velocity components, provided the relation between the upstream and downstream wave vectors $\boldsymbol{k}^U$ and $\boldsymbol{k}^D$ is known; this will be derived shortly. Although the spatial coordinates of the upstream and downstream positions do not appear explicitly, they are present implicitly through the deformation tensor so that the decomposition of the velocity field into spatial Fourier modes is assumed to be local. Stated another way, a basic assumption of the analysis is that fluid planes in the upstream flow remain fluid planes in the downstream region because of the one-to-one correspondence between upstream and downstream Fourier components. Each Fourier component assumes a sinusoidal distribution over all space, whereas the deformation tensor is a function of position. As alluded to previously, this assumption becomes more accurate as the scale decreases and should be quite adequate if the turbulence scale is small compared to the scale of the distorted flow.

Relation Between Upstream and Downstream Wave Vectors

As with $\boldsymbol{Q}^U$ and $\boldsymbol{Q}^D$, the wave vectors upstream and downstream will be related by making use of the deformation tensor. The three vectors $\boldsymbol{\Omega}$, $\boldsymbol{Q}$, and $\boldsymbol{k}$ form orthogonal systems, both upstream and downstream, with $\boldsymbol{k}$ in the direction of $\boldsymbol{\Omega} \times \boldsymbol{Q}$. The direction of Ω^U can be found from $\boldsymbol{\Omega}^D$ (which is known) using Eq. (5). The same is not true about $\boldsymbol{Q}^U$ and $\boldsymbol{k}^U$, however.

To determine the directions of the two quantities $\boldsymbol{Q}^U$ and $\boldsymbol{k}^U$, use will be made of the assumption that planes of constant phase of a vorticity wave transform to similar types of planes in moving from upstream to downstream. Thus, if the vector $\boldsymbol{\Omega}$ in Eq. (10) is replaced by $\boldsymbol{Q}$, the resulting vector (call it $\boldsymbol{A}$) on the left side will not be $\boldsymbol{Q}^U$, but it will be in the same plane as $\boldsymbol{Q}^U$ and $\boldsymbol{\Omega}^U$. Thus, the direction of $\boldsymbol{k}^U$ can be found by taking the cross product $\boldsymbol{A}$ and $\boldsymbol{\Omega}$, which will be referred to as vector $\boldsymbol{B}$. By taking the cross product $\boldsymbol{B}$ with $\boldsymbol{\Omega}^U$, the direction of $\boldsymbol{k}^U$ can be found.

The preceding discussion outlines the method for finding the direction of $\boldsymbol{k}^U$. The magnitude is found by noting that if $\boldsymbol{\Omega}$ in Eq. (10) is replaced by $\boldsymbol{k}$, the quantity on the left side (call it C) will not be $\boldsymbol{k}^U$, but the parallel planes of vorticity through the endpoints of the vector $\boldsymbol{k}^U$ (see Fig. 8). Thus, the magnitude of $\boldsymbol{k}^U$ is found by taking the product of the magnitude of $\boldsymbol{C}$ with the cosine of the angle between $\boldsymbol{C}$ and the direction of $\boldsymbol{k}^U$ determined previously. The relation between the upstream and downstream wave numbers is found to be

$$k^D/k^U = (\boldsymbol{e}_3^U)_i\, (\boldsymbol{e}_3^D)_j \frac{\partial x_i}{\partial \xi_j} \tag{12}$$

where $\boldsymbol{e}_3$ is a unit vector in the direction of the wave vector. Note that if the deformation tensor is diagonal, the velocity relationship given by Eq. (11) will reduce to results given in Ref. 16.

Numerical Results for the Rotor Face Vorticity Distribution

Computations have been carried out of the vorticity distribution at the rotor face for different flight conditions. Only a

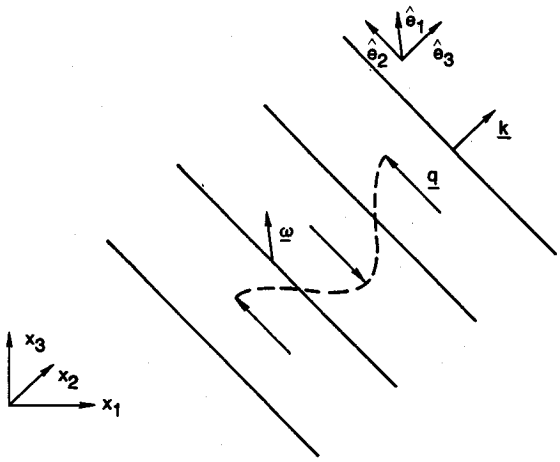

Fig. 8 Sinusoidal velocity variation for a wave vector component of turbulence; also shown are the $\hat{e}$ vectors introduced in analytical development.

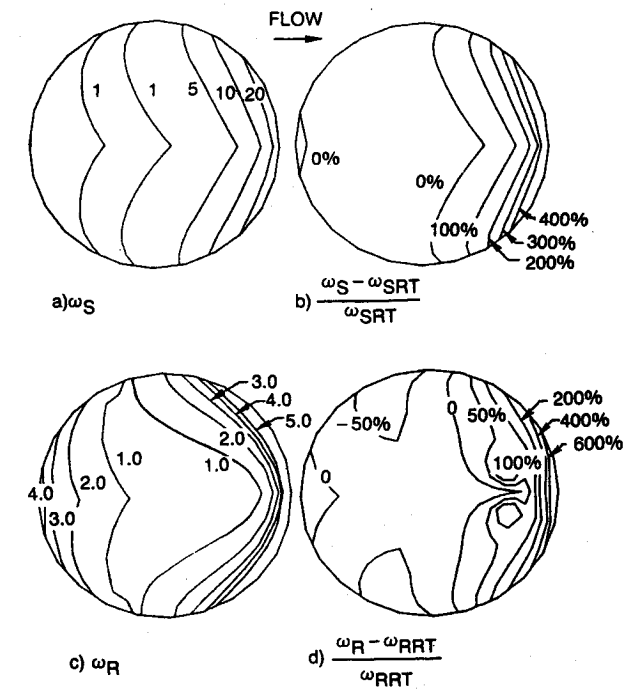

Fig. 9 Vorticity contours for hover.

portion of the results are described in the present paper, but results for all cases listed in Table 1 are given in Ref. 7. The calculations are based on isotropic turbulence as the upstream ambient condition.

Figures 9 and 10 show contours of different components of vorticitiy at the rotor face. All values are normalized by the value of the upstream vorticity component, ω_x (or ω_y or ω_z since the turbulence field upstream is isotropic).

Each figure has four parts, a-d. Part a shows the normalized local streamwise component of vorticity, i.e., the component of vorticity along the local streamwise direction.

The b part of each figure shows comparisons of the streamwise vorticity, calculated using the present analysis with that calculated based only on streamline contraction (neglecting differential drift). This is denoted by ω_{RT} since this was the approach used by Ribner and Tucker in Ref. 16. Large

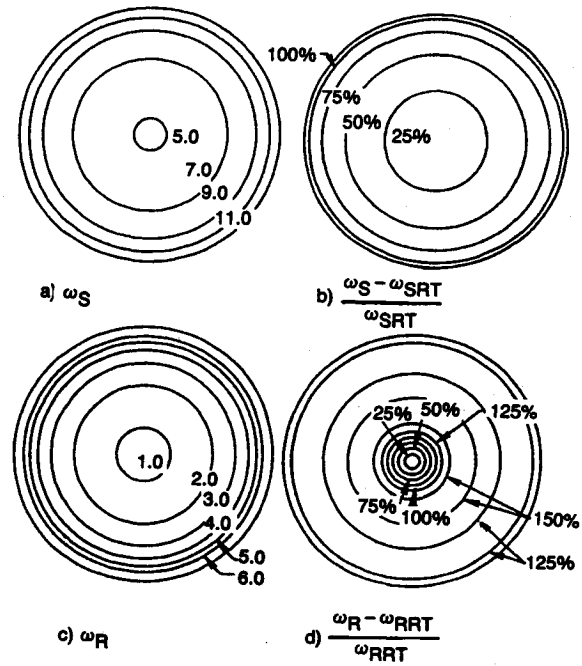

Fig. 10 Vorticity contours for low-speed vertical ascent.

changes in the shapes of the contours from a to b imply strong qualitative differences in the behavior of the streamwise vorticity as computed by the two different analyses.

Parts c and d show contours of the normalized vorticity in the plane of the rotor. They can be regarded as giving a qualitative indication about the turbulence ingestion noise since this vorticity component, which induces velocity fluctuations normal to the rotor blades, is the primary cause of the noise. Parts c and d thus provide a picture of the regions of greatest noise generation.

Considering the hover case in Fig. 9a, a large difference in drift time exists between the streamlines that enter the rotor disk on the "windward" half (the left side) and those that enter on the "lee" half. This is reflected in the large values of the streamwise vorticity on the right side of the disk. The theory, limited to stream-tube area change, gives results that are much more axisymmetric so that there are substantial differences in the relative values of the streamwise vorticity shown in Fig. 9b.

The behavior of the component of vorticity in the rotor plane also shows magnitude differences of approximately a factor of 2 between the results of the present analysis and those obtained neglecting the differential drift as well as qualitative differences in the shapes of the contours. These differences indicate that the noise predicted using the two theories could also be significantly different.

Similar trends, although less pronounced are seen in the low-speed vertical ascent case in Fig. 10. As inferred from the plots of the streamlines and time lines,[7] there are appreciable differences near the edges of the disk (Figs. 10a and 10b) between the vorticity components calculated using the present analysis and that accounting for stream-tube contraction only.

Although not shown in the present paper, the component of vorticity in a plane normal to the local streamwise direction has also been calculated and is given in Ref. 7. (This is the vector sum of the components of vorticity along the binormal and normal directions.) There are smaller differences between this component for the two analyses because its value is determined by effects that are basically local in character (i.e., streamline spacing) rather than by effects that are dependent on the time history, as is the case for the streamwise vorticity.

Finally, in the higher speed cases, there is less contraction of the stream tubes and less difference in drift time. As would be expected, therefore, changes in the predicted values of the

components of vorticity at the rotor disk between the two theories are also small.

Summary and Conclusions

1) An analytical procedure has been developed to predict helicopter rotor noise generation due to ingestion of atmospheric turbulence. The analysis combines several different models that describe the fluid mechanics of the turbulence and the ingestion process.

2) The mean flow and turbulence statistics associated with the atmospheric boundary layer have been modeled including effects of atmospheric stability length, wind speed, and altitude.

3) For the atmospheric conditions encountered by a helicopter main rotor, the turbulence field of interest can be modeled as isotropic and locally stationary and homogeneous.

4) Streamline curvature and stream-tube contraction in the rotor inflow distort the upstream turbulence so that the turbulence field at the rotor disk is nonisotropic.

5) The turbulence distortion process can be modeled as a deformation of vortex filaments (which represent the turbulence field) by a mean rotor inflow. Using a rapid distortion theory approach, the filaments are numerically tracked along the mean-flow streamlines to find the turbulence at the rotor disk plane.

6) For large mean-flow contraction ratios, accurate predictions of turbulence vorticity components at the rotor face requires incorporating the differential drift of fluid particles on adjacent streamlines.

7) Failure to account for the preceding effect also leads to substantial differences in the predicted nonisotropic and nonhomogeneous turbulence field at the rotor face. As is described in the companion paper,[1] this can lead to pronounced differences in the broadband as well as discrete tone amplitudes.

Acknowledgment

This work was conducted under NASA Langley Research Center Contract NAS1-17096.

References

[1]Amiet, R. K., Simonich, J. C., and Schlinker, R. H., "Rotor Noise Due to Turbulence Ingestion, Part II—Aeroacoustic Results," *Journal of Aircraft*, Vol. 27, Jan. 1990, pp. 15–22.

[2]George, A. R., "Helicopter Noise: State-of-the Art," *Journal of Aircraft*, Vol. 15, Nov. 1978, pp. 707–715.

[3]Brooks, T. F., and Schlinker, R. H., "Progress in Rotor Broadband Noise Research," *Vertica*, Vol. 7, No. 4, 1983, pp. 287–307.

[4]Teunissen, H. W., "Characteristics of the Mean Wind and Turbulence in the Planetary Boundary Layer," *UTIAS Review*, Vol. 32, Univ. of Toronto Institute for Aerospace Studies, Toronto, Ontario, Canada, Oct. 1970, pp. 1–46.

[5]Snyder, W. H., "Guideline for Fluid Modeling of Atmospheric Diffusion," Environmental Protection Agency, Washington, DC, Fluid Modeling Rept. 10, April 1981.

[6]Fairall, C. W., Davidson, K. L., Schacher, G. E., "A Review and Evaluation of Integrated Atmospheric Boundary-Layer Models for Maritime Applications," Naval Postgraduate School Rept. NPS-63-81-004, Nov. 1981.

[7]Simonich, J. C., Amiet, R. K., Schlinker, R. H., and Greitzer, E. M., "Helicopter Rotor Noise Due to Ingestion of Atmospheric Turbulence," NASA CR-3973, May 1986.

[8]Egolf, T. A., and Landgrebe, A. J., "Helicopter Rotor Wake Geometry and Its Influence in Forward Flight—Vol. I.—Generalized Wake Geometry," NASA CR-3726, Oct. 1983; also "Volume II—Wake Geometry Charts," NASA CR-3727, Oct. 1983.

[9]Landgrebe, A. J., and Egolf, T. A., "Rotorcraft Wake Analysis for the Prediction of Induced Velocities," U.S. Army Air Mobility Research and Development Laboratory, Fort Eustis, VA, USAAMRDL TR-74-45, Jan. 1976.

[10]Lighthill, M. J., "A Simple Fluid-Flow Model of Ground Effect on Hovering," *Journal of Fluid Mechanics*, Vol. 93, Aug. 1979, pp. 781–797.

[11]Kuchemann, D., and Weber, J., *Aerodynamics of Propulsion*, McGraw-Hill, New York, 1953, pp. 305–310.

[12]Castles, W., Jr., and De Leeuw, J. H., "The Normal Component of the Induced Velocity in the Vicinity of a Lifting Rotor and Some Examples of Its Application," NACA TR-1184, 1953.

[13]Shampine, L. F., and Gordon, M. F., *Computer Solution of Ordinary Differential Equations: The Initial Value Problem*, Freeman, San Francisco, 1975.

[14]Ribner, H. S., and Tucker, M., "Spectrum of Turbulence in a Contracting Stream," NACA TR-1113, 1953, pp. 305–310.

[15]Batchelor, G. K., and Proudman, I., "The Effect of Rapid Distortion of a Fluid in Turbulent Motion," *Quarterly Journal of Mechanical and Applied Mathematics*, Vol. 7, Pt. 1, 1954, pp. 83–103.

[16]Goldstein, M. E., "Unsteady Vortical and Entropic Distortions of Potential Flows Around Arbitrary Obstacles," *Journal of Fluid Mechanics*, Vol. 89, Dec. 1978, pp. 433–468.

[17]Goldstein, M. E., and Durbin, P. A., "The Effect of Finite Turbulence Spatial Scale on the Amplification of Turbulence by a Contracting Stream," *Journal of Fluid Mechanics*, Vol. 98, 1980, pp. 473–508.

[18]Hunt, J. C. R., "A Theory of Turbulent Flow Round Two-Dimensional Bluff Bodies," *Journal of Fluid Mechanics*, Vol. 61, Dec. 1973, pp. 625–706.

[19]Hunt, J. C. R., "A Review of the Theory of Rapidly Distorted Turbulent Flows and its Applications," *Fluid Dynamics Transactions*, Vol. 9, edited by W. Fiszdon, et al., 1978, pp. 121–152.

[20]Batchelor, G. K., *An Introduction to Fluid Dynamics*, Cambridge Univ. Press, Cambridge, England, UK, 1967, Chap. 5.